FISEVIER

Contents lists available at ScienceDirect

Electrochemistry Communications

journal homepage: www.elsevier.com/locate/elecom



Short communication

Electroactive decomposition products cause erroneous intercalation signals in sodium-ion batteries



Sophia E. Lee, Maureen H. Tang*

Department of Chemical and Biological Engineering, Drexel University, Philadelphia, PA 19104, United States

ARTICLE INFO

Keywords: Sodium-ion batteries Electroanalytical chemistry Electrolyte decomposition

ABSTRACT

Three-electrode configurations allow targeted studies of reaction mechanisms, including charge storage in and interphase formation on electrode materials for emerging sodium-ion batteries. However, using sodium metal as a reference electrode results in spontaneous formation of electroactive soluble decomposition products in an ester-based electrolyte. These electrolyte decomposition products undergo oxidation at carbon electrodes at potentials that can be mistaken for reversible sodium (de)intercalation, thus obscuring true measurements of material properties.

1. Introduction

Interest in sodium ion batteries as a low cost and earth-abundant alternative to lithium has grown dramatically in recent years [1]. However, more work is needed to understand and control the mechanisms of charge storage and solid electrolyte interphase (SEI) formation on carbonaceous electrodes [2,3]. Effective study of storage and degradation mechanisms requires an appropriate experimental system that isolates the processes of interest. For testing materials, two-electrode coin- or pouch-cells, in which a single surface acts as both the counter and reference electrode, are favored for their simplicity and direct correlation to full cell performance. However, it is difficult to distinguish between reactions at the working and counter electrode [4,5]. A three-electrode configuration that separates the counter and reference electrode is therefore preferred for mechanistic studies.

2. Experimental

2.1. Electrode fabrication

SU-8 2007 photoresist (MicroChem) was applied to a p-type boron-doped silicon wafer by spin-coating and exposing to UV light at $225\,\mathrm{mJ/cm^2}$ to induce cross-linking. Pyrolysis under ultra-high purity argon gas (Airgas) was carried out in a two-step process similar to the one used by Madou et al. [6]. Films were heated at a rate of $10\,^\circ\mathrm{C/min}$ to $300\,^\circ\mathrm{C}$ and held for $30\,\mathrm{min}$ to reduce thermal stress and then carbonized at $1000\,^\circ\mathrm{C}$ for $1\,\mathrm{h}$ and cooled to room temperature under gas flow.

Propylene carbonate (PC) (99.7%) from Sigma-Aldrich was dried with 4 Å molecular sieves for a minimum of 72 h to remove any trace water content. Sodium perchlorate (\geq 98.0%), Tetrabutylammonium perchlorate (TBAP) (\geq 99.0%), and silver nitrate (\geq 99.0%) from Sigma-Aldrich were used as received.

2.3. Electrochemical measurements

Electrochemical experiments were carried out in a custom PTFE compression cell [7] in a three-electrode configuration with 1 M sodium perchlorate in PC as electrolyte. Sodium metal was used as the counter electrode with a fine porosity frit (Chemglass) and with sodium metal or commercial silver ion electrode as the reference. Sodium electrodes were made by wrapping a small amount of sodium metal (99.9%, Sigma-Aldrich) around the stripped end of an insulated copper wire. Commercial silver ion electrode (Basi, Inc.) had a filling solution of 10 mM silver nitrate in PC with 100 mM TBAP as supporting electrolyte. The leak rate of silver ions measured by atomic absorption spectroscopy was $3.8\times 10^{-8}\,\mu\text{mol/h},$ so there is little risk from cross-contamination (S.E. Lee and M.H. Tang, in preparation). Cells were cycled using cyclic voltammetry (CV) with a BioLogic VSP-300 potentiostat between 0.015 and 2.7 V vs Na/Na⁺ at scan rates between 0.2 and 10 mV/s. All working electrodes underwent an initial formation of 5 cycles at 2 mV/ s. Automatic IR compensation at 85% was applied based on electrochemical impedance spectroscopy at 100 KHz and values ranged from 400 to 600Ω , primarily due to the silicon substrate. Cycling of bare

E-mail address: mhtang@drexel.edu (M.H. Tang).

^{2.2.} Materials

^{*} Corresponding author.

silicon wafers showed background anodic and cathodic currents of $<0.06\,\mu\text{A/cm}^2$ and $1\,\mu\text{A/cm}^2$ respectively, indicating that sodium is not alloying with the crystalline silicon and that the carbon film is responsible for the majority of electrolyte decomposition.

2.4. Characterization

X-ray photoemission spectroscopy (XPS) measurements were performed with a Versa Probe 5000 spectrometer (Physical Electronics Inc., USA) with monochromatic Al K α radiation and a beam setting of 100 μ M with 25 W and 15 kV. Peaks were assigned to 284.5, 286, 287.5 and 288.7 eV for C–C, C–O, C=O and O–C=O respectively. Raman spectroscopy measurements were performed with an inVia Confocal Raman Spectrometer (Renishaw, UK) with an 514 nm Ar laser. Peaks were assigned to 1598, 1355, 1525 and 1210 for G, D, M1 and M2 respectively using Gaussian peaks [8].

3. Results and discussion

In order to better understand the competing mechanisms of SEI formation and charge storage, we have developed a model system for the targeted study of surface interactions using thin films of hard carbon in a three-electrode configuration. The thin-film geometry eliminates complications from conductive additive or polymer binder and isolates surface interactions between the electrode and electrolyte from bulk behavior. Films were characterized using XPS and Raman to show similarity to other hard carbon materials. The XPS spectra (Fig. 1a) shows an oxygen-to-carbon ratio of approximately 10% and the C1s shows a strong sp² carbon peak with a mix of C-O, C=O and O-C=O groups in small quantities, resembling spectra for hard carbon from a variety of sources. Raman (Fig. 1b) shows an I_d/I_G ratio of 1.84 for pristine carbon, indicating a significant degree of disorder.

During initial CV scans at $2\,\text{mV/s}$ low reversible oxidation is observed, with a reversible capacity around $0.5\,\mu\text{Ah/cm}^2$ and coulombic efficiency between 15 and 25%, consistent with other pyrolyzed carbon films [9]. After decreasing the scan rate to $0.2\,\text{mV/s}$, a growing oxidation peak between 0.5 and 1 V is observed during the anodic sweep. Subsequently, the anodic current increases with scan rate as shown in Fig. 2a and b. Finally, during a second $2\,\text{mV/s}$ sweep, anodic current increases by approximately six-fold for total oxidative charge capacity of $3\,\mu\text{Ah/cm}^2$. Thus, the observed electrode behavior shifts from purely irreversible reduction at the surface to apparent reversible reduction and oxidation as a result of slow scan rate cycling.

Two hypotheses can explain this hysteresis. In the first, a bulk change to the carbon structure increases the reversible capacity. This could occur if at moderate scan rates (e.g. $2\,\text{mV/s}$) sodium diffusion is too slow for appreciable sodium intercalation [9], but slow scan rates (e.g. $0.2\,\text{mV/s}$) permit intercalation and modify the hard carbon structure. Similar pre-intercalation treatments have been used to improve transport in other battery materials [10]. To investigate this hypothesis, structural changes were evaluated through XRD and Raman. XRD (not shown) was inconclusive due to the low thickness and crystallinity of the film. Although Raman shows a small change in the ratio of disordered to graphitic carbon, the change was insufficient to support the structural hypothesis (Fig. 1b).

An alternative explanation for the hysteresis originates in the instability of the sodium reference electrode. Ponrouch et al. have reported multiple cases in which increased resistance and potential drift at the reference electrode leads to changes in the measured behavior of the sodium metal plating reaction [5,11]. When the slow scan rate cycling is repeated with a silver-ion reference electrode, as shown in Fig. 2c, d, there is no shift in oxidation behavior with scan rate. While there is a slight increase in oxidation current at 2 mV/s, this can be attributed to slight roughening of the surface, and is significantly less than the increase observed for a sodium reference electrode. The lack of hysteresis here indicates that the effect of scan rate is caused by changes

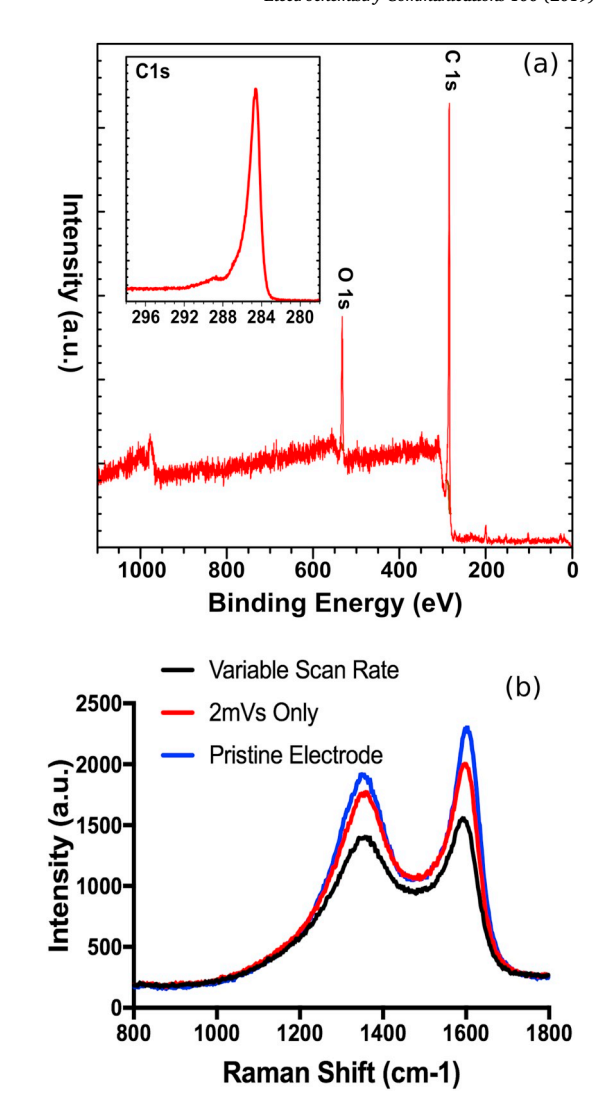


Fig. 1. (a) XPS survey spectrum and C1s elemental scan (inset) for pristine carbon thin film electrode. (b) Raman spectra for pristine carbon thin film electrode (blue), electrode cycled at 2 mV/s (red), and at multiple low scan rates (black). (For interpretation of the references to color in this figure legend, the reader is referred to the web version of this article.)

not to the carbon working electrode, but rather to the sodium reference electrode. To further investigate the effect of the sodium reference electrode on the measured current, the sodium reference is replaced with a silver-ion reference after completing the slow scan rate cycling (Fig. 3). The cycling behavior is unchanged after substituting reference electrodes (Fig. 3c), indicating that the increased oxidation is not from a resistive sodium reference electrode. However, removing the electrolyte from the cell and replacing it with fresh electrolyte (Fig. 3d) decreases the oxidation current to the original value, where it remains over five cycles of additional cycling at 2 mV/s. These results indicate that electroactive degradation products are formed by electrolyte reduction at the surface of the sodium reference electrode and are able to migrate or diffuse to the working electrode where they are oxidized. While it is unclear why the counter electrode does not contribute to erroneous signals when the reference electrode is replaced by silver-ion, it is possible that current passed at the counter electrode results in local oxidation of degradation products, thus preventing them from diffusing to the working electrode.

The solubility of reduction products from sodium metal electrodes has been well documented in literature, as indicated by the development of a yellow color in the electrolyte and the detection of soluble

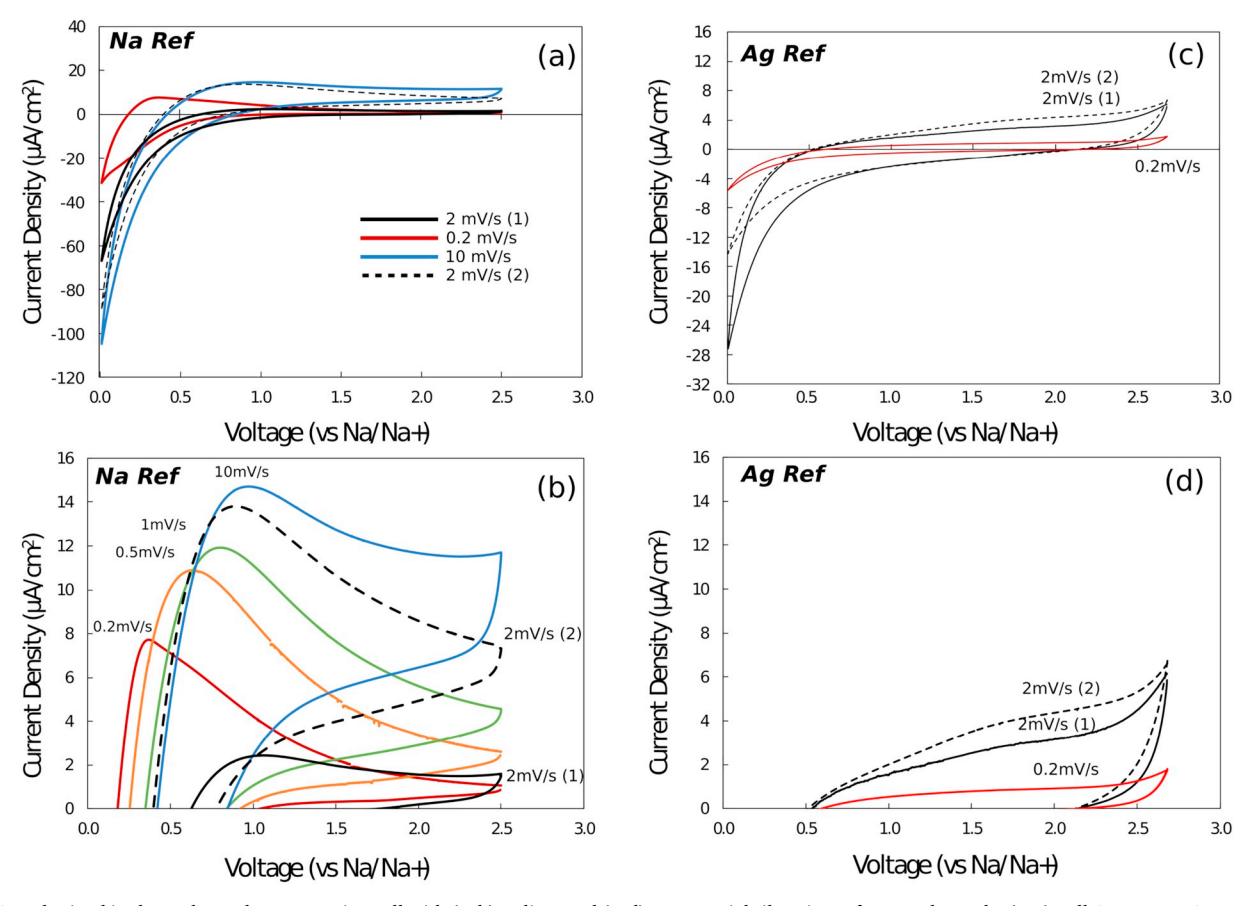


Fig. 2. CVs obtained in three-electrode compression cell with (a, b) sodium and (c, d) commercial silver-ion reference electrode. (a, c) Full CV scans at 2 mV/s prior to additional cycling (solid black), at 0.2 (red) and 10 mV/s (blue), and 2 mV/s after cycling (dashed black). (b) Anodic portion of CV scans with sodium reference, at 2 mV/s prior to additional cycling, at 0.2, 0.5, 1, and 10 mV/s respectively, and 2 mV/s after cycling. (d) Anodic portion of CVs with silver-ion reference electrode, during initial cycling at 2 mV/s (solid black), at 0.2 mV/s (red), and on subsequent 2 mV/s scan (dashed black). (For interpretation of the references to color in this figure legend, the reader is referred to the web version of this article.)

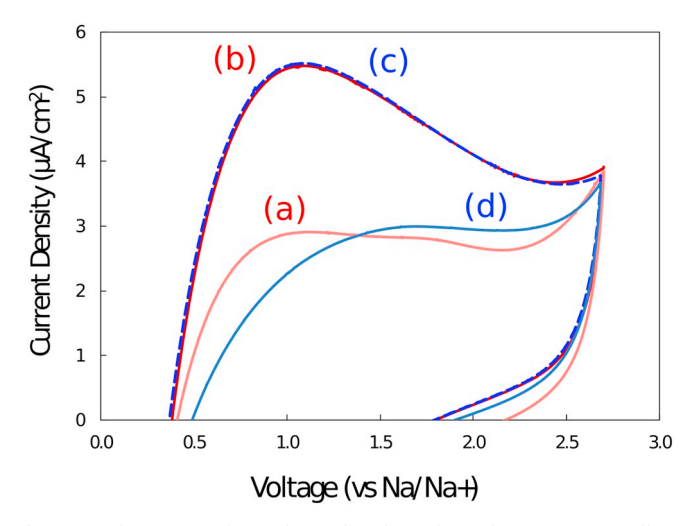


Fig. 3. Anodic portion of CVs obtained in three-electrode compression cell. (a, b) Using sodium reference electrode during (a) initial cycling at $2\,\text{mV/s}$ and (b) at $2\,\text{mV/s}$ after slow scan cycling. (c, d) In same cell, using silver-ion reference electrode during $2\,\text{mV/s}$ cycling with (c) same electrolyte as sodium metal cycles and (d) with pristine electrolyte.

products in solution via GC-MS and FT-IR [12–15]. Bommier et al. showed with FTIR that the spectrum for cycled electrolyte resembles that of the surface of sodium metal soaked in electrolyte, indicating that degradation products from the sodium metal electrode are solubilized

in electrolyte [12]. Dugas et al. have previously proposed that additional capacity upon discharge could be attributed to the oxidation of soluble products from the counter electrode [16], and Komaba et al. showed that degradation products could be oxidized at voltages above 2.8 V vs Na/Na $^+$ [15]. Our work demonstrates clearly that these products are oxidized at lower than previously reported potentials, down to 1 V vs sodium metal, and are not limited to counter electrode products.

4. Conclusions

While the instability of degradation products at sodium metal counter electrodes has been demonstrated in two-electrode half-cells, the results here show that the use of sodium metal as the reference electrode in a three-electrode system can also obscure phenomena at the working electrode. Most critically, signals associated with electrolyte degradation product oxidation can be confused with intercalation reactions inherent to the working electrode. As these currents can yield incorrect conclusions regarding electrode-electrolyte interactions, caution should be applied when using sodium metal, either as a counter electrode in two-electrode set-ups or as a reference electrode in three-electrode tests. After testing a number of alternatives, including a variety of intercalation and alloying electrode materials, (S.E. Lee and M.H. Tang, in preparation) we propose the non-aqueous silver/silver ion electrode as a reliable alternative for use in three-electrode tests.

Notes

The authors declare no competing financial interest.

Acknowledgements

The authors thank Cassie Lees for help with XRD and Mallory Clites for help with Raman. This work was carried out in part at the Singh Center for Nanotechnology, and at the Drexel Central Research Facilities. This work was supported by the National Science Foundation [grant number 1607991]; The Singh Center for Nanotechnology is supported by the NSF National Nanotechnology Coordinated Infrastructure Program [grant number NNCI-1542153].

References

- [1] N. Yabuuchi, K. Kubota, M. Dahbi, S. Komaba, Chem. Rev. 114 (2014) 11636–11682, https://doi.org/10.1021/cr500192f.
- [2] S.W. Zhang, et al., Energy Storage Mater. 3 (2016) 18–23, https://doi.org/10.1016/j.ensm.2015.12.004.
- [3] C. Bommier, X. Ji, Small (2018) 1703576, https://doi.org/10.1002/smll. 201703576
- [4] A. Rudola, D. Aurbach, P. Balaya, Electrochem. Commun. 46 (2014) 56–59, https://doi.org/10.1016/j.elecom.2014.06.008.
- [5] D.S. Tchitchekova, et al., J. Electrochem. Soc. 164 (2017) A1384-A1392, https://

- doi.org/10.1149/2.0411707jes.
- [6] C. Wang, G. Jia, L.H. Taherabadi, M.J. Madou, J. Microelectromech. Syst. 14 (2005) 348–358, https://doi.org/10.1109/JMEMS.2004.839312.
- [7] Y. Yamada, Y. Iriyama, T. Abe, Z. Ogumi, Langmuir 25 (2009) 12766–12770, https://doi.org/10.1021/la901829v.
- [8] E. De La Llave, et al., Isr. J. Chem. 55 (2015) 1260–1274, https://doi.org/10.1002/ ijch.201500064.
- [9] F. Kong, et al., Electrochem. Solid-State Lett. 1 (1998) 39–41, https://doi.org/10. 1149/1.1390628.
- [10] M. Clites, E. Pomerantseva, Energy Storage Mater. 11 (2018) 30–37, https://doi. org/10.1016/S0378-7753(01)00588-2.
- [11] D.I. Iermakova, R. Dugas, M.R. Palacín, A. Ponrouch, J. Electrochem. Soc. 162 (2015) A7060–A7066, https://doi.org/10.1149/2.0091513jes.
- [12] C. Bommier, et al., Adv. Mater. Interfaces 3 (2016) 1600449, https://doi.org/10. 1002/admi.201600449.
- [13] S. Komaba, et al., Adv. Funct. Mater. 21 (2011) 3859–3867, https://doi.org/10. 1002/adfm.201100854.
- [14] G.G. Eshetu, et al., ChemSusChem 9 (2016) 462–471, https://doi.org/10.1021/am200973k.
- [15] S. Komaba, et al., ACS Appl. Mater. Interfaces 3 (2011) 4165–4168, https://doi. org/10.1021/am200973k.
- [16] R. Dugas, et al., J. Electrochem. Soc. 163 (2016) A2333–A2339, https://doi.org/10. 1149/2.0981610jes.